Proceedings of the ASME 2016 Pressure Vessels and Piping Conference
PVP2016
July 17-21, 2016, Vancouver, British Columbia, Canada

PVP2016-63345

DIRECT OBSERVATION OF ELASTIC AND PLASTIC STRAIN FIELDS DURING DUCTILE TEARING OF A FERRITIC STEEL

Harry E. Coules
University of Bristol
Bristol, UK
harry.coules@bristol.ac.uk

Graeme C. M. Horne
Frazer-Nash Consultancy Ltd.
Bristol, UK
g.horne@fnc.co.uk

Matthew J. Peel
University of Bristol
Bristol, UK
matthew.peel@bristol.ac.uk

Sam J. Oliver
University of Bristol
Bristol, UK
sam.oliver@bristol.ac.uk

Derreck G. A. Van Gelderen
University of Bristol
Bristol, UK
d.vangelderen@bristol.ac.uk

Thomas Connolley
Diamond Light Source
Didcot, Oxfordshire, UK
thomas.connolley@diamond.ac.uk

ABSTRACT

Residual and thermal stresses have a considerable effect on the process of brittle fracture. In addition to this, the effect of these stresses on elastic-plastic fracture is known to be significant. This is accounted for in structural integrity assessment methodologies such as R6 Rev 4 and BS 7910:2013 by introducing factors representing the interaction between primary and secondary stresses (those that do and do not contribute towards plastic collapse, respectively).

The initiation of ductile tearing in a ferritic pressure vessel steel was studied experimentally. Energy-dispersive X-ray diffraction was used to determine lattice strains in the vicinity of a crack tip in modified compact tension specimens at incremental loading steps until the initiation of ductile tearing. The X-ray diffraction measurements allowed the stress field to be evaluated with a high spatial resolution. At the same time, the pattern of total strain at the surface of the specimen was observed using digital image correlation. Prior to the experiment, two samples were subjected to localised out-of-plane compression ahead of the crack tip to introduce a residual stress field and hence significant crack loading in the absence of external load. Stress and strain field data for cracked specimens, with and without a pre-existing residual stress field, indicated significant differences in the development of plastic strain up to the point of tearing initiation. It is shown that this can only be explained when both residual stress and prior material hardening are taken into account.

INTRODUCTION

Residual stress in engineering materials strongly affects brittle fracture but has a diminished influence on ductile fracture. During the loading of a crack or defect in an elastic-plastic material, any pre-existing residual stress field is affected by plastic deformation and therefore is partially relaxed at the point of fracture initiation. This diminishing effect has been demonstrated experimentally in several recent studies involving residual stress measurement of fracture specimens [1–3]. To account for this, structural integrity assessment procedures such as R6 Rev. 4 [4] and BS 7910:2013 [5] often contain simplified methods for predicting the combined effect of residual and applied stresses on fracture initiation. These procedures are both essentially J-integral estimation schemes with additional failure safeguards and are inherently conservative. However, this conservatism could be potentially reduced with a better understanding of the relative contributions of primary and secondary stress to crack driving force.

In the elastic-plastic fracture regime, the parameter J characterises the energy release rate for a crack in a nonlinear elastic material and is often used as a criterion to predict fracture initiation in common engineering materials. It may be calculated using the path integral [6]:

$$J = \int_{\Gamma} \left(W \delta_{1i} - \sigma_{ij} \frac{\partial u_j}{\partial x_1} \right) n_i \, ds \qquad (1)$$

where W is the volumetric strain energy density, u_j and σ_{ij} are the displacement and stress fields, respectively, and ds is an increment of path length on the closed contour Γ, which surrounds the crack tip, for which n_i is an outward-facing normal vector. In the presence of thermal or residual stresses, an additional term is required in Equation 1 to preserve the contour-independent nature of the result [7]:

$$J_{mod} = \int_{\Gamma} \left(W\delta_{1i} - \sigma_{ij} \frac{\partial u_j}{\partial x_1} \right) n_i \, ds + \int_{A} \left(\sigma_{ij} \frac{\partial \varepsilon_{ij}}{\partial x_1} - \frac{\partial W}{\partial x_1} \right) dA \quad (2)$$

where A is the area inside Γ and ε_{ij} is the (total) strain. This allows the energy release rate to be characterised even in the presence of residual stress and prior plastic strain. In a truly elastic-plastic material, the strain energy density term W must be carefully defined. It now represents the sum of elastic strain energy and energy dissipated by irreversible plastic deformation. Additionally, if initial strain and hence residual stress is present the effect of initial strain on W must be excluded, so W is now defined as [7]:

$$W = \int_0^{\varepsilon_{ij}^m} \sigma_{ij} \, d\varepsilon_{ij}^m \quad (3)$$

where ε_{ij}^m is any portion of elastic or plastic strain not considered part of the initial strain state ε_{ij}^0 in the uncracked body:

$$\varepsilon_{ij} = \varepsilon_{ij}^0 + \varepsilon_{ij}^m. \quad (4)$$

In this work we examine the use of the modified J-integral J_{mod} (Equation 2) to characterize the crack-driving force in the presence of residual stress in a real ductile material. For this purpose, the elastic and total strain fields surrounding a notch tip up to and during the initiation of ductile tearing in specimens of ferritic steel were mapped at high spatial resolution and compared with results from finite element analysis of the same process. These measurements allow the effect of combined applied and residual stress on fracture to be studied in detail.

Modified Compact Tension (C(T)) specimens of a ductile ferritic steel with and without pre-existing residual stress fields were loaded incrementally up to the initiation of ductile fracture. During this loading, Energy-Dispersive X-ray Diffraction (EDXD) was used to measure the development of the stress field and Digital Image Correlation (DIC) was used to observe the total strain field. These measurements were compared with predictions of stress/strain development in the specimens made using Finite Element Analysis (FEA). This allowed J_{mod} values to be compared for the residually-stressed and non-residually-stressed specimens.

EXPERIMENTAL

Modified compact tension specimens of the ferritic pressure vessel steel BS 1501–224 28B were prepared: first, four 62.5 × 60 × 5 mm rectangular steel coupons were produced. Two of these coupons were indented in the region ahead of the (future) notch tip using a pair of 8 mm diameter cylindrical tool steel compression punches applied using a compressive load of 75 kN. Three coupons (one indented) were then cut into C(T) specimens using wire Electrical Discharge Machining (EDM). The C(T) specimens were not fatigue pre-cracked, but simply notched using wire EDM, in order that the notch tip could be placed at a precise location relative to the pre-existing residual

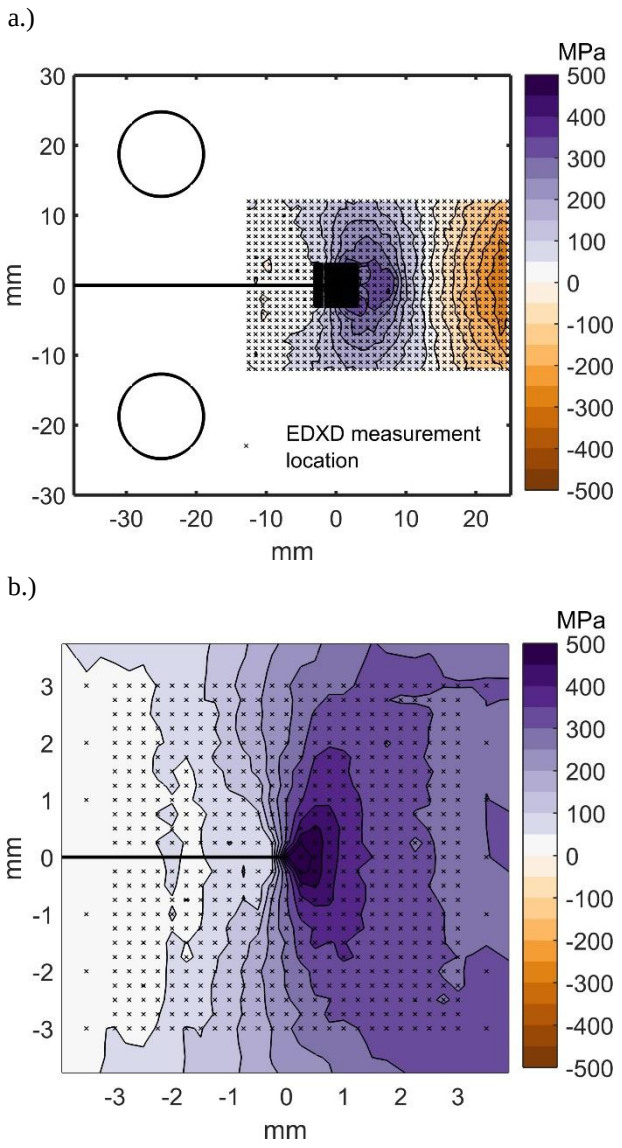

Figure 1: EDXD measurement locations on the C(T) specimens. a.) General distribution of measurement locations, b.) region of measurements at a higher spatial resolution around the notch tip. Crack-transverse component of stress shown.

stress field in the indented specimen. The indentation and notching procedures were designed to create opening-mode secondary loading of the notches. The notch tips were approximately semi-circular with a radius of 101±3 μm prior to the experiment.

Fracture loading of the C(T) specimens was carried out on the I12 beamline [8] at the Diamond Light Source (Oxfordshire, UK). During loading, I12 was used in energy-dispersive diffraction mode to map the elastic strain field within the specimens. At each loading step, strain measurements were taken at 1575 measurement points on the specimen, with a spatial resolution of 1 mm over a large area of the specimen and with a higher resolution of 0.25 mm in a 6 × 6 mm square region surrounding the notch tip (Figure 1). The collimated beam resulted in an elongated measurement volume of 0.2 × 0.2 × 6 mm, encompassing the entire specimen thickness, but geometrically biased towards the centre of specimen. For each point, I12's energy-dispersive X-ray detector was used to obtain diffraction spectra in 23 different directions, each rotated around the beam (and hence the sample normal) by an angle ϕ. Each spectrum was recorded in q-space (q=2π/d, where d is the lattice spacing of the reflection) and contained the first 5 ferrite *hkl* reflections. Peaks were fitted using a Gaussian function to give the peak position q_ϕ^{hkl}. The strain in a given direction for a given (*hkl*) is:

$$\varepsilon_\phi = \frac{(q_0^{hkl} - q_\phi^{hkl})}{q_0^{hkl}} = p_{11}\sigma_{11} + p_{12}\sigma_{12} + p_{22}\sigma_{22} \qquad (5)$$

where $q_0^{hkl}$is the peak position for the same reflection obtained from a stress-free reference sample and $p_{ij}$are the stress factors. Setting $\phi = 0$ for the vertical detector element gives:

$$p_{ij} = \begin{cases} \frac{1}{2}S_2 h_i^2 + S_1 \; if \; i = j \\ 2.\frac{1}{2}S_2 h_i h_j \; if \; i \neq j \end{cases} \quad where \; h = \begin{bmatrix} \cos\phi \\ \sin\phi \end{bmatrix} \qquad (6)$$

where $S_1, 1/2S_2$ are *hkl* dependent diffraction elastic constants. One equation is produced for each reflection in each direction. Solving the resulting system of equations allows for the determination of the in-plane components of stress in a single measurement, but without sensitivity to out-of-plane stresses. Diffraction elastic constants were determined by taking EDXD measurements from a uniaxial tension specimen of the same material at several increments of stress in the elastic regime.

In addition to the diffraction measurements, 3D Digital Image Correlation (DIC) was used to measure the total strain development on the surface of each specimen during loading. A speckle pattern, consisting of a white basecoat with black speckles approximately 5 pixels across, was created on each specimen using spray paint. The speckle pattern on the specimen was observed using a two-camera (8-bit 4 Megapixel) Dantec Dynamics Q400 DIC system [9]. The cameras were mounted on the loading machine with separation and standoff distances of about 250 mm, such that the C(T) specimens filled the frames of both cameras. Total strain on the surface of the specimen in the in-plane directions was calculated by comparing the images to reference images taken prior to loading using a subset size of 25 pixels and the inbuilt 9×9 local regression smoothing algorithm, based on the adaptive spline polynomial algorithm, such that strains had a contribution from both subset deformation and displacement gradient.

The three C(T) specimens were subjected to the loading paths shown in Figure 2. Specimens 2 & 3 were loaded monotonically up to the initiation of tearing, while Specimen 1 had additional unload-reload steps. Specimen 1, which did not contain an initial residual stress, was used to examine the residual stress fields which occurred during these load-unload-reload cycles. X-ray radiography of the crack tip was used detect tearing initiation (see Figure 5).

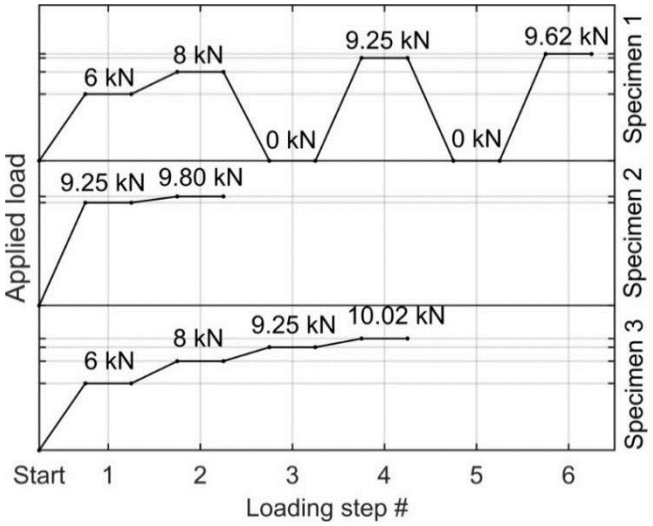

Figure 2: Loading paths for the three C(T) specimens. EDXD and DIC measurements were taken at each loading step.

MODELLING

Finite element analysis of the C(T) specimens following the loading paths shown in Figure 2 was performed. For the indented specimen it was necessary to model the indentation process and cutting of the notch which occurred prior to the fracture loading. Mechanical constitutive properties of the steel were derived from uniaxial tensile test results. The material was modelled using incremental plasticity theory and was assumed to exhibit isotropic hardening. Visco-plastic behaviour was observed in the steel during tensile testing and tests at different loading rates were carried out. The uniaxial stress/strain curve at a loading rate of 50 μm/min (over a specimen parallel length of 80 mm) was

judged to approximate the quasi-static properties of the material, and so results for this loading rate were used to derive the material properties used in the models.

All of the finite element analysis was performed using the Abaqus/Standard v6.12 solver [10] with a mesh of 8-noded linear brick elements. Focussed mesh regions surrounding the crack tip (see Figure 3a) were used to ensure accuracy of the model in the presence of the large gradient in plastic deformation expected here, and to allow contour integral evaluation over fixed-radius paths. 6-noded linear wedge elements were used at the crack tip. J-integral values were extracted from the calculated stress/strain fields using the equivalent domain integral method described by Shih et al. [11]. Since the specimens were nominally symmetric only one quarter of the specimen was modelled, with appropriate boundary conditions applied on the plane of the crack and at the mid-thickness. J-integral evaluation for the residually-stressed specimen was performed using the method described by Lei [12]. After simulation of the indentation process, the resulting residual stress and hardening state data were transferred into a separate model of crack introduction and loading using the Abaqus *INITIAL CONDITIONS keyword, with the stress data imported using the FILE parameter, and the hardening state data specified explicitly. A plot of the residual stress distribution in a specimen prior to notch introduction is shown in Figure 4.

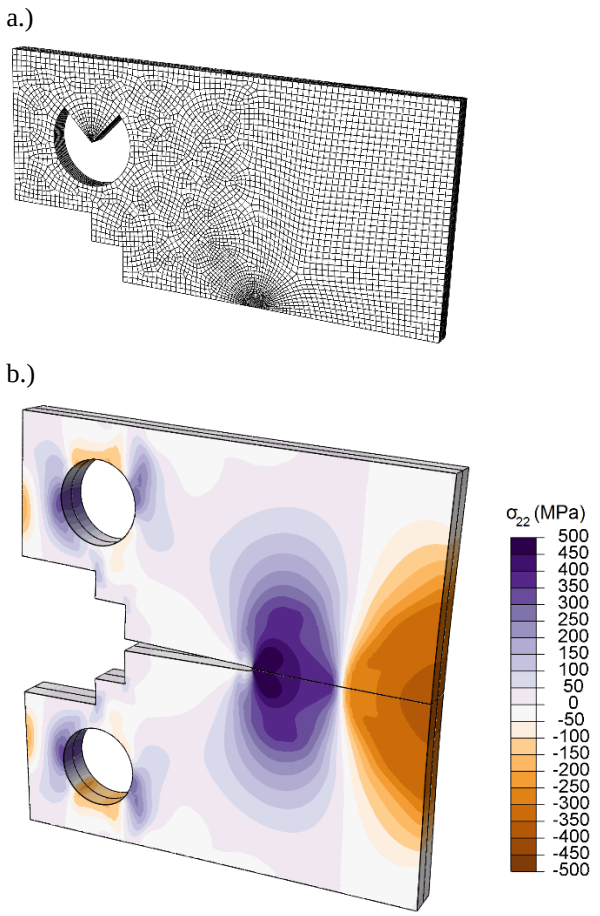

Figure 3: Modelling of Specimen 1. a.) Finite element mesh, b.) stress field (crack-transverse component shown) at an applied load of 9.25 kN.

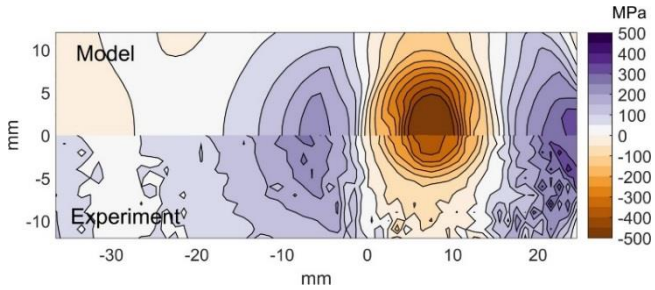

Figure 4: Residual stress field in an indented C(T) specimen prior to introduction of the notch.

RESULTS & DISCUSSION

For the final step in its loading trajectory, each C(T) specimen was loaded under displacement-controlled conditions until tearing initiation. The X-ray images in Figure 5 show the approximately semi-circular tip of the initial EDM notch, blunting of the notch during loading, and finally the initiation of ductile tearing. Figures 6-8 show the measured and modelled stress in the crack transverse direction, in the three specimens, for the loading levels shown in Figure 2.

The compression process creates a residual stress field which, after the introduction of the notch, causes opening-mode notch loading. This is shown in the 0 kN image in Figure 8: a region of strongly tensile stress in the crack-transverse direction is created, along with a region of compressive stress further ahead in the indented region. Good agreement is observed between the stress fields measured using EDXD and those predicted using the finite element method. However, it is important to note two key differences. Firstly, on the load relaxation steps (0 kN post 8 kN and 0 kN post 9.25 kN) in Specimen 1 the stress fields predicted using FEA differ slightly from those measured – more so than for measurements following monotonic loading. This difference suggests that the stress reversal which occurs during unloading is the cause of this discrepancy. The possibility of anisotropic material hardening properties and the Bauschinger effect was not taken into account in the models, so it appears likely that these effects play a measurable role in stress field development during the unload-reload cycle. Secondly, in the modelled 'tearing' load step for each specimen the zone of strongly tensile stress directly ahead of the crack tip lies slightly to the left of that observed in the experiments. The material damage and separation which occurs during the initiation of tearing in the real specimens causes relaxation of stresses at the initial tip of the notch, in turn causing the zone of highest stress to shift forward. However, since material damage was not simulated in the models, this shift does not occur in the modelling results.

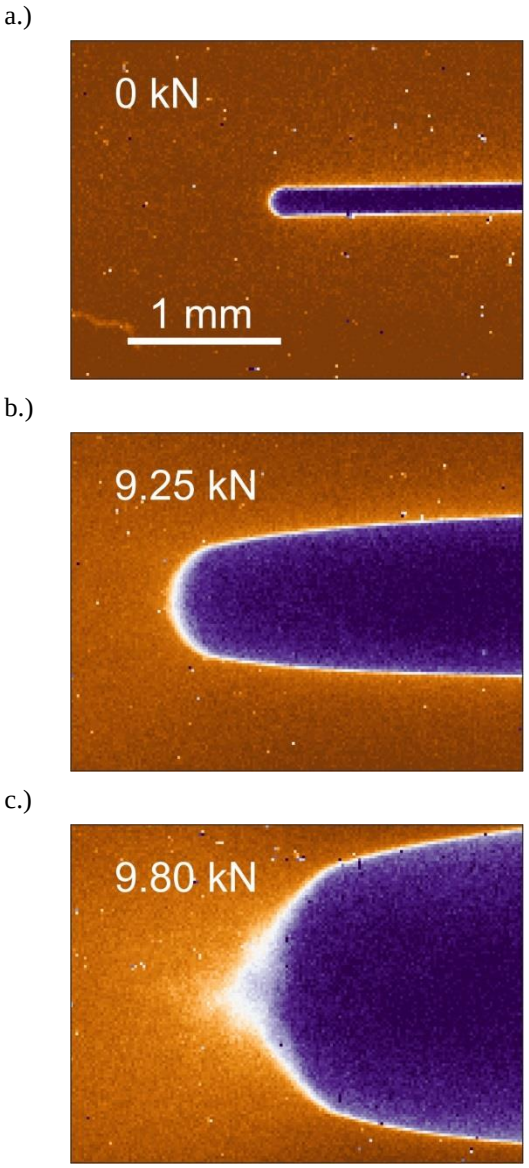

Figure 5: X-ray images of the notch tip of Specimen 2 under the different loading states shown in Figure 2. a.) The semi-circular tip of the initial EDM notch, b.) blunting of the notch during loading and c.) initiation of ductile tearing.

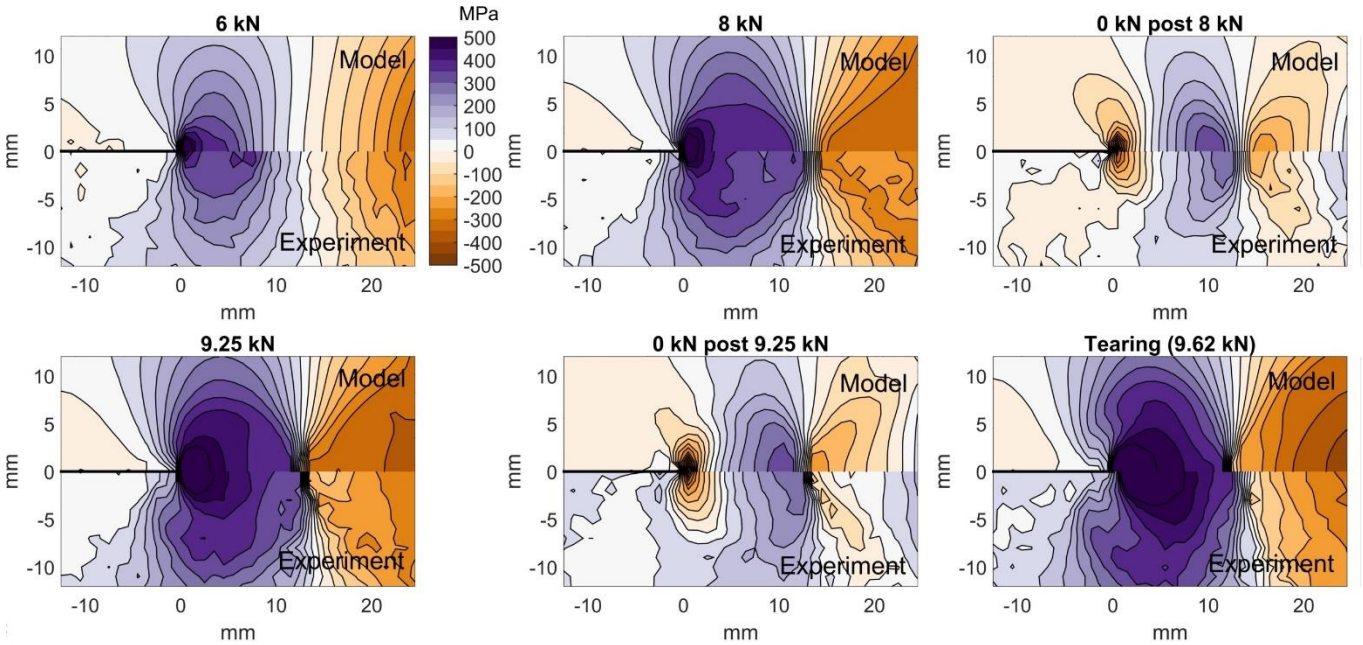

Figure 6: Stress in the crack-transverse direction (σ_{yy}) at the mid-plane of Specimen 1during the loading path shown in Figure 2. Results from both finite element analysis (Model) and EDXD (Experiment) are shown.

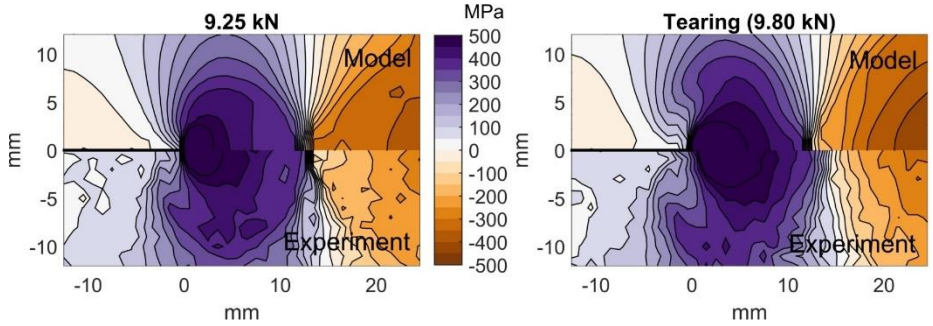

Figure 7: Stress in the crack-transverse direction (σ_{yy}) at the mid-plane of Specimen 2 during the loading path shown in Figure 2. Results from both finite element analysis (Model) and EDXD (Experiment) are shown.

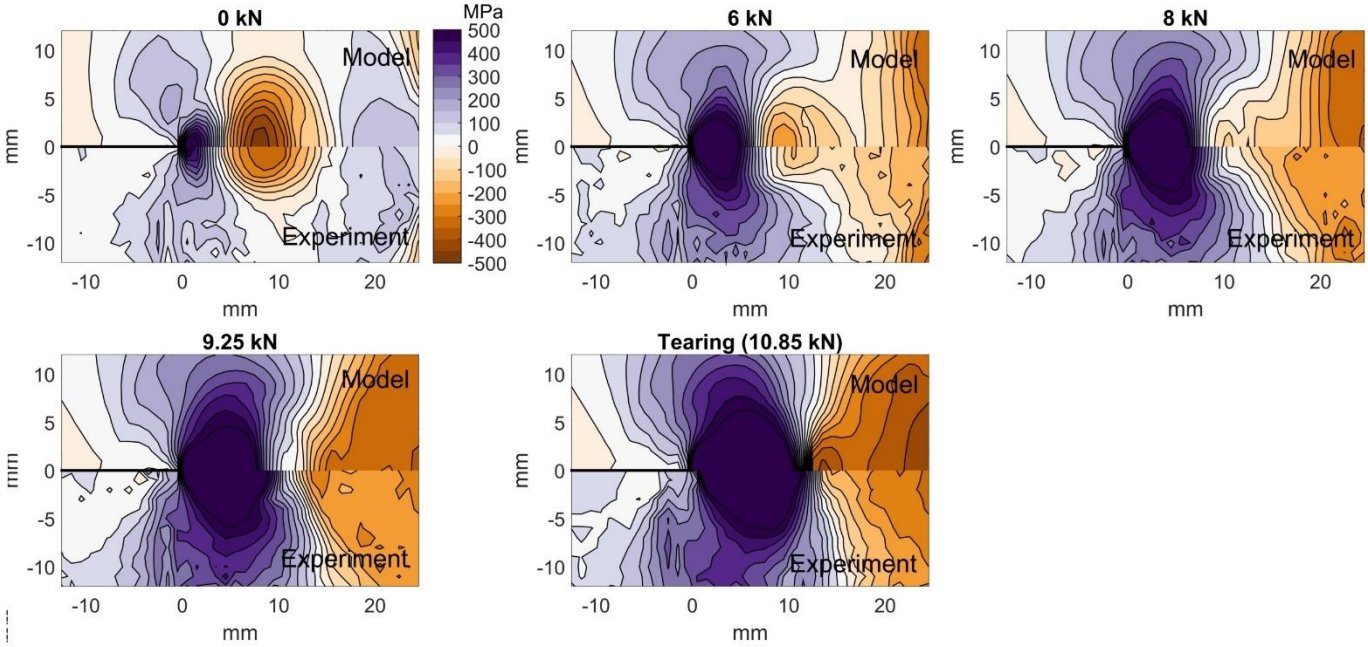

Figure 8: Stress in the crack-transverse direction (σ_{yy}) at the mid-plane of Specimen 3 during the loading path shown in Figure 2. Results from both finite element analysis (Model) and EDXD (Experiment) are shown.

One difficulty that arises in using the J-integral to analyse fracture in the presence of residual stresses relates to the amount of information required to calculate J-integral explicitly. The type of measurements demonstrated here can be used to address this problem in two ways. Firstly, they can be used as part of a combined approach in which finite element results are used to calculate J, having first been validated using experimental data. Secondly, with certain limitations they could be used to calculate J explicitly. Here, the first approach has been adopted and J and J_{mod} are calculated from the finite element analysis results. To calculate the modified J-integral, the method described previously by Lei was used [12], with the distributions of residual stress and hardening mapped from a model of the indentation process onto one incorporating notch introduction and loading using the Abaqus *INITIAL CONDITIONS keyword. Using this method, the Abaqus/Standard v6.12 solver takes the initially-specified stress state to be residual. Particular care should be taken when using solver versions 6.11 and later with RESIDUAL STRESS STEP, as detailed by Lei [12], as it may not produce the correct behaviour. Path independence of the calculated results should also be checked.

For all of the specimens at each load level, J varied along the notch tip line in the through-thickness direction. However, in all cases the most severe loading condition occurs at then specimen mid-thickness. The J-integral results were use to calculate the equivalent elastic-plastic stress intensity factor K_J assuming approximately plane stress conditions using the equation:

$$K_J = \sqrt{JE} \qquad (7)$$

where E is the Young's modulus of the material. In all cases, the J-integral results were calculated using large integration domains such that the results were seen to reach stabilized 'far-field' values. Results of the crack driving force calculations are shown in Figure 9.

Prior to fracture loading, the notch in the indented specimen is acted upon by residual stress, and so there is a finite crack-driving force at zero load (see Figure 9). At a load of 6 kN, the crack driving force for the indented specimen is still higher than that for the non-indented specimen, as residual stress acts in combination with the applied load. However, at an applied load of 8 kN significant plasticity in the region surrounding the crack tip greatly diminishes the effect of residual stress and so the crack-driving force for the two cases at this load level is similar.

In addition to residual stress, the indentation process also causes strain-hardening of material in and around the indented region. This prior hardening starts to affect the development of the stress and strain fields during loading as plasticity occurs. It therefore affects the crack-driving force more at higher applied load levels. In Figure 9, additional curves are plotted to show the values of K_J for a theoretical specimen containing the residual stress distribution introduced by indentation but not the corresponding distribution of material hardening, and a theoretical specimen containing the hardening distribution introduced by indentation but no residual stress. At higher levels of applied load (9.25, 10.56 and 10.85 kN) where plasticity becomes widespread, the effect of prior hardening acts to reduce K_J and this effect exceeds the residual stress field's diminishing influence on K_J. Consequently, at the point of tearing initiation in the non-indented specimens, an indented specimen with the same applied

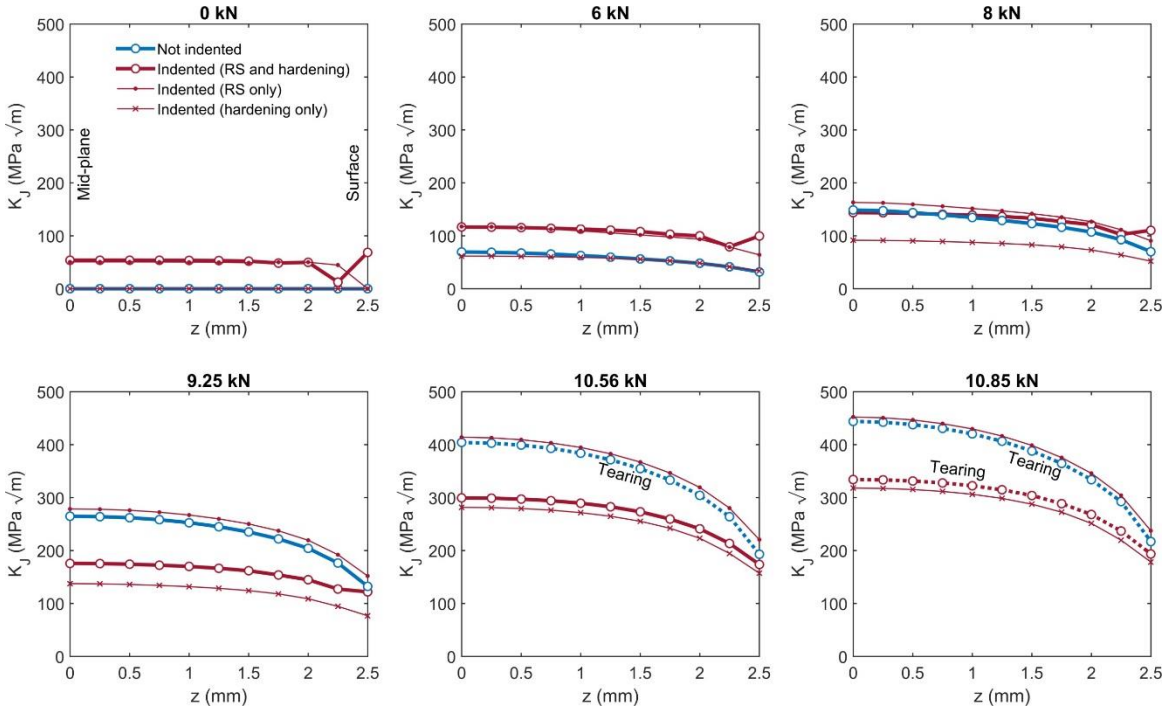

Figure 9: Elastic-plastic equivalent stress intensity factor K_J as a function of the through-thickness dimension z in indented and non-indented specimens, calculated using FEA. The theoretical results for specimens containing only the residual stress distribution caused by indentation (but no material hardening), and only the material hardening state (but no residual stress), are also shown. Dashed lines indicate tearing observed.

load would experience a significantly lower elastic-plastic crack driving force. The effect of prior material hardening can be observed directly in the distributions of total strain shown in Figure 10. The indented specimen (Figure 10c) shows greatly reduced surface deformation in both the models and the experiment in comparison with the other two specimens. While the combination of a low-constraint crack/notch geometry and a ductile specimen material made the effect of prior hardening large in this experiment, in conditions of more limited plasticity it would be less significant. However, this highlights the importance of considering both the presence of residual stress and differences in a material's hardening state when predicting elastic-plastic fracture.

CONCLUSIONS

In this work we have experimentally mapped a residual stress field acting on a notch, and monitored stress field development during loading and ductile fracture. Using finite element analysis of the side punching and the loading history – validated from these measurements – it was shown that for the specimens tested, the residual stress field no longer contributes significantly to driving fracture at high levels of applied load prior to tearing initiation, but that material's initial hardening state becomes very important by comparison. Therefore, when considering the fitness-for-service of a component containing residual stress, it is important to consider the process that caused the residual stress field and the corresponding hardening state of the material. These observations also expose the potential pitfall of modelling residual stresses by introducing an initial thermal deformation, which does not capture the material hardening state.

ACKNOWLEDGMENTS

Access to the I12 beamline was provided by Diamond Light Source under proposal number EE11463. We dedicate this work to our late friend and mentor Prof. David Smith, who also helped to plan these experiments.

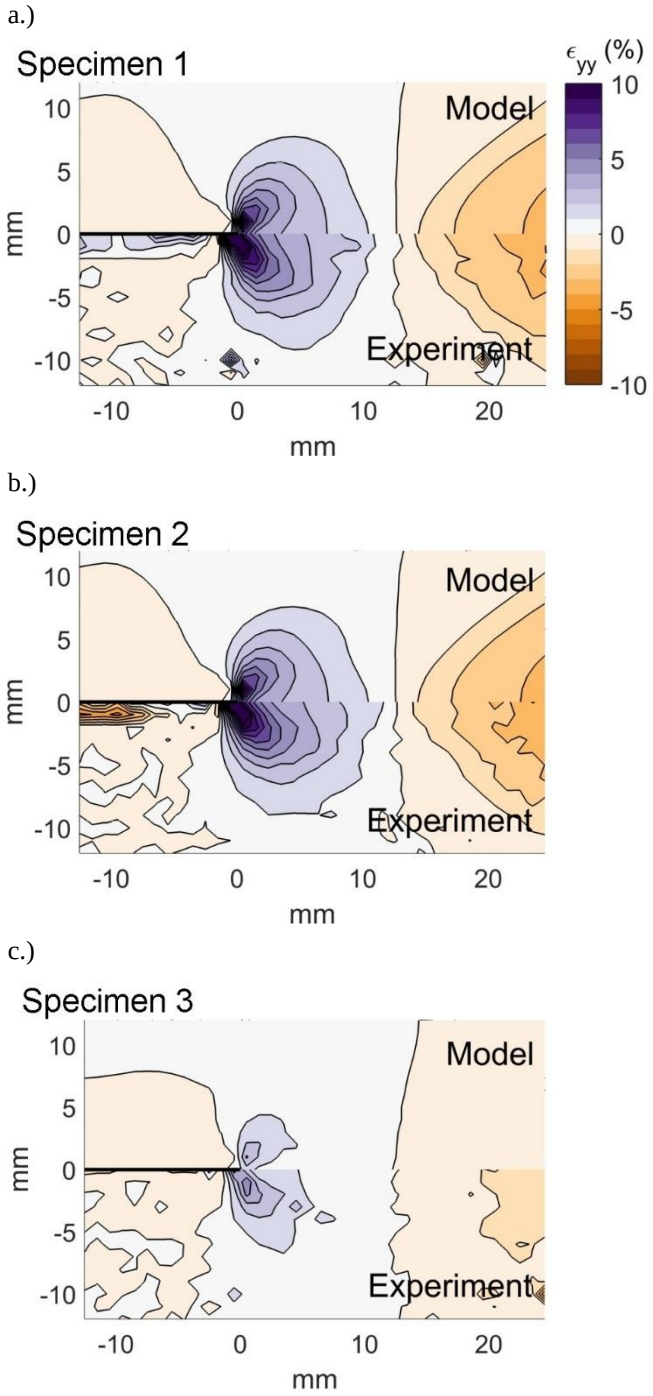

Figure 10: Distribution of total strain at the surface of the specimens in the region surrounding the notch at an applied load of 9.25 kN. The crack-transverse component of total strain (ε_{yy}) relative to the material state prior to loading is shown. "Model" indicates finite element analysis results and "Experiment" indicates digital image correlation results.

REFERENCES

[1] T. Bolinder and J. Faleskog, "Evaluation of the influence of residual stresses on ductile fracture," *Journal of Pressure Vessel Technology, Transactions of the ASME*, vol. 137, no. 6, p. 061408, 2015.

[2] A. Mirzaee-Sisan, C. E. Truman, D. J. Smith, and M. C. Smith, "Interaction of residual stress with mechanical loading in an austenitic stainless steel," *Fatigue and Fracture of Engineering Materials and Structures*, vol. 31, no. 3–4, pp. 223–233, 2008.

[3] A. Mirzaee-Sisan, C. E. Truman, D. J. Smith, and M. C. Smith, "Interaction of residual stress with mechanical loading in a ferritic steel," *Engineering Fracture Mechanics*, vol. 74, no. 17, pp. 2864–2880, 2007.

[4] *R6: Assessment of the Integrity of Structures Containing Defects, Revision 4, Amendment 10*. EDF Energy, Gloucester, 2013.

[5] *BS 7910:2013 - Guide to methods for assessing the acceptability of flaws in metallic structures*. BSi, 2013.

[6] J. R. Rice, "A path independent integral and the approximate analysis of strain concentration by notches and cracks," *Journal of Applied Mechanics*, vol. 35, pp. 379–386, 1968.

[7] Y. Lei, "J-integral evaluation for cases involving non-proportional stressing," *Engineering Fracture Mechanics*, vol. 72, no. 4, pp. 577–596, 2005.

[8] M. Drakopoulos, T. Connolley, C. Reinhard, R. Atwood, O. Magdysyuk, N. Vo, M. Hart, L. Connor, R. Humphreys, G. Howell, S. Davies, T. Hill, G. Wilkin, U. Pedersen, A. Foster, N. D. Maio, M. Basham, F. Yuan, and K. Wanelik, "I12: the Joint Engineering, Environment and Processing (JEEP) beamline at Diamond Light Source," *Journal of Synchrotron Radiation*, vol. 22, pp. 828–838, 2015.

[9] *Q-400 System Istra 4D Software Manual*. Dantec Dynamics GmbH, Skovlunde, Denmark: , 2014.

[10] *Abaqus/Standard v6.12*. Providence, RI, USA: Dassault Systemes Simulia Corp., 2012.

[11] C. F. Shih, B. Moran, and T. Nakamura, "Energy release rate along a three-dimensional crack front in a thermally stressed body," *International Journal of Fracture*, vol. 30, no. 2, pp. 79–102, 1986.

[12] Y. Lei, "J Calculation for a crack in a welding residual stress field following a FE welding simulation," in *Transactions of SMiRT 23 Manchester, United Kingdom - August 10-14, 2015*, 2015, p. 213.